# Biofilms mechanically damage epithelia by buckling.

Alice Cont, Tamara Rossy, Zainebe Al-Mayyah, Alexandre Persat*

Institute of Bioengineering and Global Health Institute, School of Life Sciences, Ecole Polytechnique Fédérale de Lausanne, Lausanne, Switzerland

*alexandre.persat@epfl.ch

**Abstract**

During chronic infections and in microbiota, bacteria predominantly colonize their hosts as multicellular structures called biofilms. Biofilms form when single cells divide while embedding themselves in an elastic matrix of extracellular polymeric substance, protecting resident cells from external stressors and coordinating collective behaviors[1]. While we understand how biofilms form in vitro, we still lack a basic understanding of how they interact with tissues in vivo, and ultimately how they influence host physiology. A common assumption is that biofilm-dwelling bacteria biochemically interact with their hosts, for example by secreting toxins[2]. However, the contributions of mechanics, while being central to the process of biofilm formation, have been vastly overlooked as a factor influencing host physiology. Here we show that biofilms mechanically damage epithelia by transmitting of internally-generated forces to host tissue. By combining tissue-engineering and biomechanical measurement techniques, we found that forces generated by *Vibrio cholerae* biofilms can disrupt host epithelia by breaking epithelial cell-cell junctions and attachment to extracellular matrices. We demonstrate that biofilms from *V. cholerae* and *Pseudomonas aeruginosa* can similarly induce large deformations of soft synthetic hydrogels. Using traction force microscopy, we demonstrate that friction between the biofilm and the hydrogel surface generates internal mechanical stress that cause biofilms to buckle. Matrix components that maintain the mechanical cohesion of biofilms promote buckling, while those

that maintain surface adhesion transmit buckling stress to the substrate. Altogether, our results demonstrate that forces generated by bacterial communities play an important role not only in biofilm morphogenesis but also in host physiology, suggesting a mechanical mode of infection.

To explore how biofilms form within their hosts, we engineered epithelial monolayers of Caco-2 cells on a soft extracellular matrix (ECM) (**Fig. 1A**). This produces soft and tight ECM-adherent epithelia that reproduce the mechanical properties of real tissues. We seeded the surface of these epithelia with *V. cholerae* expressing constitutively high levels of cyclic-di-GMP (Vc WT*), which forms robust biofilms and has reduced virulence[3]. Biofilms formed at the epithelial surface within 20 h (**Fig. 1B-D**). Overall, biofilms perturbed the shape of the epithelium. Under biofilms, the cell monolayer detached from its ECM substrate and was often bent (**Fig. 1B-ii**). In other instances, Caco-2 cells lost cohesion and were engulfed by the biofilm. This allowed the biofilm to breach the epithelium and contact the ECM. There, biofilms deformed the ECM substrate, turning the initially flat surface into a dome-like shape (**Fig. 1B-iv**). These disruptions did not depend on host cell type as *V. cholerae* could also damage and bend monolayers of MDCK cells which has strong cell-cell junctions[4] (**Fig. 1C**). Our observations suggest that biofilms apply mechanical forces on host tissue that can perturb the morphology and integrity of epithelia, as well as the underlying ECM.

To test whether and how biofilms disrupt epithelia, we sought to decouple the effect of mechanics from host cell biological response by exploring their formation on soft axenic substrates. We generated ~100 µm-thick polyethylene glycol (PEG) hydrogel films in microchannels, thus enabling high resolution live confocal imaging of biofilm formation under flow (**Fig. 2A**). On soft hydrogels, *V. cholerae* formed biofilms whose bottom surfaces appeared bell-shaped, consistent with what we observed on epithelial monolayers and ECM

(**Fig. 2B**), but in striking difference with the typically flat-growing biofilms forming on glass. To test whether this shape was a result of hydrogel deformation, we embedded fluorescent tracer particles within the hydrogel film. We could observe that biofilms in fact deformed hydrogels as the fluorescent tracer particles filled the apparent bell-shaped void at its core (**Fig. 2C**). We also found that biofilms of *P. aeruginosa*, an opportunistic pathogen that forms robust airway epithelial biofilms during chronic pneumonia, could similarly deform soft PEG hydrogels (**Fig. 2D-E, Fig. S1**). Therefore, *V. cholerae* and *P. aeruginosa* both deform the substrate, consistent with a force-driven mechanism that is independent of their respective biofilm architecture and the composition of their extracellular polymeric substance (EPS).

How could biofilms mechanically deform their substrates? Bacterial colonies wrinkle on agar plates due to internal mechanical stress generated by simultaneous expansion and friction[5]. In biofilms, this also causes internal stresses influencing the spatial organization of single cells within *V. cholerae* biofilms[6,7]. Friction force between the microcolony and the surface opposes biofilm expansion, generating an inward internal stress that leads to a buckling instability verticalizing or reorienting contiguous cells[7,8]. We thus reasoned that biofilm could deform soft substrates by transmission of internal stresses to the substrate they grow on. To demonstrate this, we performed dynamic visualizations of hydrogel film deformations and recorded the surface profiles for multiple biofilms. By radial re-slicing and averaging around the biofilm centers, we could extract the deformation profile $\delta$, its maximum deformation amplitude $\delta_{max}$ and full-width at half maximum $\lambda$ (**Fig. 3A**). By reconstructing hydrogel surfaces for biofilms of different sizes, we found that $\delta_{max}$ and $\lambda$ linearly scaled with the diameter *d* of the biofilm (**Fig. S2**), indicating that biofilm expansion promotes surface deformation. We went further by tracking these deformations over time for single biofilms. Deformations increased as biofilms grew, even showing a slight recess near the biofilm edges reminiscent of higher order buckling modes (**Fig. 3B-C, Movie S1**)**.** In these visualizations, we noticed that there was a lag between the increase in biofilm diameter and the onset of deformation, with a finite deformation only appearing after 7 h of

growth. This was further confirmed by following the deformations generated by many biofilms, as finite in plane deformations mainly appeared after 6 to 7 h of growth (**Fig. 3D**). Rescaling by the diameter of the biofilm collapsed $\delta_{max}$ measurements, highlighting a critical biofilm diameter (35 µm) above which deformations emerged (**Fig. 3E**). The existence of a critical diameter is reminiscent to buckling instabilities of rigid bodies subject to compressive stress, as in Euler buckling. Also consistent with an Euler-type buckling instability, the width of the deformation scales linearly with biofilm diameter[9].

To further support our model where biofilm buckling drives surface deformations, we investigated how bacterial growth applied forces on the hydrogel. We therefore tracked the displacements of the fluorescent particle tracers embedded within the hydrogel in 3D with a digital volume correlation algorithm. Specifically, the hydrogel displacement field shows that the biofilm pushes the hydrogel radially before reaching the critical diameter, in the outward direction (**Fig. 3F** and **Fig. S4**). These deformations result from the opposition between growth and friction between cells and the surface, and generate an internal force within the biofilm oriented radially towards its center, which ultimately causes the biofilm to buckle.

We then wondered whether forces driving deformations could break epithelial cell-cell junctions and disrupt monolayers. To answer this question, we directly measured the forces generated by the biofilm on the hydrogel films by traction force microscopy. Traction forces were surprisingly large, reaching 5 MPa in the biofilm center after 12 h of growth (**Fig. 3G**). In comparison, cell-cell junctions break when experiencing a few kPa [10]. Therefore, biofilms produce sufficient force to mechanically dismantle epithelia. We note that the magnitude of the stress is relatively large for a biological structure of this size. This stress is in essence generated by the expansion of single bacterial cell, itself driven by turgor pressures can reach the MPa range[11].

Given the large forces generated by biofilms on substrates, we wondered to which extent they could deform different types of tissues. To test this, we reproduced the mechanical properties of various tissue types by tuning the stiffness of the PEG hydrogel films between

10 kPa and 200 kPa [12,13]. The rate of increase of the deformation amplitude was inversely correlated with stiffness, resulting in differences in $\delta_{max}$ between colonies of identical diameter growing on substrates with distinct stiffnesses **(Fig. 3H)**. For each stiffness, the deformation amplitude $\delta_{max}$ and the width $\lambda$ increased linearly with biofilm diameter (**Fig. 3I** and **Fig. S3**). Stiff hydrogels only slightly deformed, recapitulating the morphology of glass-grown biofilms. In contrast, biofilms growing on soft hydrogels displayed large deformations **(Fig. 3I)**. Rescaling $\delta_{max}$ with the biofilm diameter highlights a power-law relationship between deformation and substrate stiffness qualitatively consistent with the theory of buckling of plates coupled to an elastic foundation (**Fig. S5**)[14].

We then identified biofilm components regulating force generation and transmission, particularly focusing on EPS matrix components. The *V. cholerae* matrix is composed of a polysaccharide and proteins, including Rbma which is responsible for cell-cell cohesion and Bap1 which promotes biofilm-surface adhesion[15]. We found that biofilms of *rbmA* deletion mutants were unable to deform the hydrogel substrate, demonstrating that cell-cell cohesion is an essential ingredient in force generation (**Fig. 4A**). Interestingly, biofilms of *bap1* deletion mutants grew slightly bent but delaminated from the substrate which remained flat, thereby creating a gap between the biofilm and the hydrogel (**Fig. 4A**). This demonstrates that adhesion between the biofilm and the substrates transmits normal mechanical stress. In a similar manner, mutation in EPS matrix components of *P. aeruginosa* reduced but did not abolish deformations (**Fig. 4B**). *P. aeruginosa* secretes the polysaccharides Pel and Psl, and the protein CdrA, all of which play a role in maintaining viscoelastic properties of the biofilm[16–18]. Deletion mutants in *psl, pel* and *cdrA* showed a decrease in deformation amplitude, further demonstrating that mechanical cohesion plays a key role in surface deformation (**Fig. 4B-C**). Since *P. aeruginosa* does not possess a dedicated matrix component for substrate adhesion, we grew biofilms on hydrogels with large Young's modulus to increase the relative contribution of adhesion and elastic energy of the substrate[19]. Consistent with our buckling-adhesion model, these biofilms delaminated (**Fig.**

**4D**). In summary, cell-cell mechanical cohesion is essential in generating the internal stress that promotes biofilm buckling, while cell-substrate adhesion transmits this stress to the underlying substrate (**Fig. 4E**).

We found that biofilms can cause damage to epithelial tissues by buckling, causing delamination or rupture of intercellular junctions, suggesting that biofilms could mechanically damage host tissues. In fact, biofilms commonly cause tissue lesions. For example the urine of vaginosis patients contains desquamated epithelial cells covered with biofilms[20,21]. Also, commensal biofilms form scabs at the epithelial surface of honeybee's gut, triggering immune responses [22]. Epithelial integrity is also commonly compromised in intestinal diseases such as inflammatory bowel disease, while being highly influenced by the microbiota[23]. Finally, hyper-biofilm forming clinical variants of *P. aeruginosa* causes significant damage to the surrounding host tissue despite its reduced virulence[24]. Mechanical interactions between bacterial collectives and their host may thus represent an overlooked contributor of infections and dysbiosis.

**Acknowledgements**

We would like to thank the Fitnat Yildiz, Matt Parsek, Melanie Blokesch and Bonnie Bassler for strains and plasmids and John Kolinski and Pedro Reis for discussions.

**Funding**

This work was supported by the Swiss National Science Foundation Projects Grant 31003A_169377, the Gabriella Giorgi-Cavaglieri Foundation, the Gebert Rüf Stiftung and the Fondation Beytout.

**Competing interests**

None

## Materials and Methods

*Cell culture*

Caco-2 cells and MDCK cells were maintained in T25 tissue culture flasks (Falcon) with DMEM medium (Gibco) supplemented with 10% fetal bovine serum at 37°C in a CO2 incubator.

*Cell culture on collagen/Matrigel gels*

To resemble the extracellular matrix natural niche, we cultured epithelial cells at the surface of collagen and Matrigel based hydrogels. Hydrogel solutions were prepared on ice to avoid premature gelation by mixing 750 µl of neutralized collagen with 250 µl of growth-factor reduced Matrigel matrix (Corning, 356231). The neutralized collagen was obtained by mixing 800 µl of native type I collagen isolated from the bovine dermis (5mg/ml, Cosmo Bio Co., Ltd.) with 10 µl of $NaHCO_3$ (1 M), 100 µl of DMEM-FBS and 100 µl of DMEM 10X. We then

spread 100 µl of the hydrogel solution in glass bottom dishes (P35G-1.5-20-C, MatTek), which were kept on ice. Excess solution was removed from the sides of the well to avoid the formation of a meniscus. To promote collagen adhesion, the wells were previously functionalized with a 2% polyethyleneimine solution (Sigma-Aldrich) for 10 min and a 0.4% glutaraldehyde solution (Electron Microscopy Science) for 30 min. We finally placed the coated dishes at 37°C in a $CO_2$ incubator for 20 minutes to allow gelation.

MDCK and Caco-2 cells were detached from the flask using trypsin (Sigma-Aldrich). We seeded the cells at a concentration of 1000 cells/mm$^2$ on top of the gels. We let the cells adhere for 1 day and then we filled the dishes with 2 ml of culture medium. The medium was changed every 2 days.

*Bacterial strains and culture conditions*

A list of the strains and plasmids is provided in **Table 1**. All strains were grown in LB medium at 37°C. Deletion of the *V. cholerae* genes *rbmA* and *bap1* were generated by mating a parental A1552 *V. cholerae* strain, rugose variant, with *E. coli* S17 strains harboring the deletion constructs according to previously published protocols [25]. *P.aeruginosa* strains (PAO1 parental strain) are all constitutively expressing GFP (attTn7::miniTn7T2.1-Gm-GW::PA1/04/03::GFP).

*Infection of tissue-engineered epithelia by Vibrio cholera*

*V. cholerae* was grown in LB medium at 37°C to mid-exponential phase (OD 0.3-0.6). Bacteria were washed 3 times by centrifugation and resuspension in Dulbecco's phosphate-buffered saline (D-PBS). The cultures were then diluted to an optical density of $10^{-7}$ and filtered (5.00 µm-pore size filters, Millex) to ensure the removal of large bacterial clumps, thereby isolating planktonic cells. This ensured that biofilms growing on epithelia formed from single cells. We loaded 200 µL of diluted culture on top of Caco-2 or MDCK cells that were cultured for 1 to 7 days post-confluence on collagen/Matrigel gels. Bacteria were

allowed to adhere to the surface for 20 minutes, after which cells were rinsed two times with D-PBS.

For the implementation of the flow on top of Caco-2 cells, we prepared a circular slab of PDMS with the same dimensions as the dish. We punched 1mm inlet and outlet ports in this PDMS slab. We then glued it to the rim of the dish, where no cells are present. We then connected the inlet port to a disposable syringe (BD Plastipak) filled with culture medium using a 1.09 mm outer diameter polyethylene tube (Instech) and a 27G blunt needle (Instech). The syringes were mounted onto a syringe pump (KD Scientific) positioned inside a $CO_2$ incubator at 37°C. The volume flow rate was set to 50 $\mu L \cdot min^{-1}$.

For stationary biofilm growth on MDCK cells, the glass bottom dishes were filled with 2 mL of culture medium and were incubated at 37°C in a $CO_2$ incubator.

*Fabrication of PEG hydrogels and mechanical characterization*

To generate PEG hydrogels films we prepared solutions of M9 minimal medium containing poly(ethylene glycol) diacrylate (PEGDA) as the precursor and lithium phenyl-2,4,6-trimethylbenzoylphosphinate (LAP, Tokio Chemical Industries) as the photoinitiator. Molecular weight and concentration of PEGDA were tuned to obtain hydrogels with different stiffnesses (**Table 2**), while the concentration of LAP is kept constant at 2 mM.

To incorporate fluorescent microparticles into the PEG hydrogels, we modified the original solution by substituting 2 µL of M9 medium with 2 µL of red fluorescent particles solution (ThermoFischer, FluoSpheres, Carboxylate-modified Microspheres, 0.1 µm diameter, 2% solids, F8887).

To prepare the samples for mechanical characterization, we filled PDMS wells (5 mm diameter, 4 mm height) with the hydrogel solution. We covered the wells with a coverslip and we let them polymerize in a UV transilluminator (Bio-Rad Universal Hood II) for 5 minutes. The resulting hydrogel cylinders were immersed in M9 overnight and tested with a rheometer (TA instruments) in compression mode, at a deformation rate of 10 µm/s. Beforehand, the diameter of the cylinders was measured with a digital caliper, while the

height of the cylinder was defined as the gap distance at which the force starts differing from zero. The elastic modulus corresponds to the slope of the linear fit of the stress-strain curves in the range of 15% strain. The final modulus is the average modulus of 3 replicates.

*Fabrication of thin PEG hydrogel layers and implementation with PDMS microfluidic chip*

We fabricated microfluidic chips following standard soft lithography techniques. More specifically, we designed 2 cm-long, 2 mm-wide channels in Autodesk AutoCAD and printed them on a soft plastic photomask. We then coated silicon wafers with photoresist (SU8 2150, Microchem), with a thickness of 350 µm. The wafer was exposed to UV light through the mask and developed in PGMEA (Sigma-Aldrich) in order to produce a mold. PDMS (Sylgard 184, Dow Corning) was subsequently casted on the mold and cured at 70 °C overnight. After cutting out the chips, we punched 1 mm inlet and outlet ports. We finally punched a 3 mm hole right downstream of the inlet port. This hole, after being covered with a PDMS piece, acts as a bubble trap.

To obtain thin and flat hydrogel layers, a drop of about 80 µL of the hydrogel solution was sandwiched between two coverslips and incubated in the UV transilluminator for 5 minutes to allow gelation. The bottom coverslip (25x60 mm Menzel Gläser) was cleaned with isopropanol and MilliQ water, while the upper one (22x40 mm Marienfeld) was functionalized with 3-(Trimethoxysilyl)propyl methacrylate (Sigma-Aldrich) following the standard procedure. In short, cleaned coverslips were immersed in a 200 mL solution of ethanol containing 1 mL of the reagent and 6ml of dilute acetic acid (1:10 glacial acetic acid:water) for 5 minutes. They were subsequently rinsed in ethanol and dried. This functionalization enables the covalent linkage of the hydrogel to the coverslip.

Right after polymerization, the coverslips were separated using a scalpel and thus exposing the hydrogel film surface. We then positioned the PDMS microfluidic chip on top of the hydrogel film. This results in a reversible, but sufficiently strong bond between the hydrogel and the PDMS, allowing us to use the chips under flow without leakage for several days. The assembled chips were filled with M9 to maintain the hydrogel hydrated.

*Biofilm growth in microfluidic chambers*

All *V. cholerae* and *P. aeruginosa* strains were grown in LB medium at 37°C until mid-exponential phase (OD 0.3-0.6). The cultures were diluted to an optical density of $10^{-3}$ and subsequently filtered (5.00 µm-pore size filters, Millex) to ensure the removal of large bacterial clumps. We then loaded 6.5 µL of the diluted bacterial culture in the channels, from the outlet port. We let them adhere for 20 minutes before starting the flow. We connected the inlet port to a disposable LB-filled syringe (BD Plastipak) mounted onto a syringe pump (KD Scientific), using a 1.09 mm outer diameter polyethylene tube (Instech) and a 27G needle (Instech). For all conditions, the volume flow rate was 10 $\mu L \cdot min^{-1}$, which corresponds to a mean flow speed of about 0.25 $mm \cdot s^{-1}$ inside the channels. The biofilms were grown at 25°C.

*Staining procedures*

Caco-2 cells and MDCK cells were incubated for 20 minutes in a 10 µM solution of CellTracker Orange CMRA (Invitrogen, C34551) and washed with DPBS before seeding the bacteria.

Since *V. cholerae* strains were not constitutively fluorescent, biofilms were incubated for 20 minutes with a 10 µM solution of SYTO9 (Invitrogen, S34854) and washed with M9 minimal medium before visualization. This results in double staining of epithelial cells in the case of infection experiments.

*Visualization*

For all visualizations, we used an Nikon Eclipse Ti2-E inverted microscope coupled with a Yokogawa CSU W2 confocal spinning disk unit and equipped with a Prime 95B sCMOS camera (Photometrics). For low magnification images, we used a 20x water immersion objective with N.A. of 0.95, while for all the others we used a 60x water immersion objective with a N.A. of 1.20. We used Imaris (Bitplane) for three-dimensional rendering of z-stack pictures and Fiji for the display of all the other images.

To obtain the deformation profiles, z-stacks of the hydrogel containing fluorescent microparticles were performed every 0.5 µm, while a brightfield image of the base of the biofilm was taken to allow measurement of the diameter of the biofilm. For the visualization of the full biofilm, z-stacks of the samples were taken every 2-3 µm. For timelapse experiments, biofilms were imaged as soon as the flow was started, while for all the other experiments biofilms were imaged between 10 and 24 h post-seeding.

*Image analysis and computation of deformation profiles*

Starting from confocal imaging pictures of the microparticle-containing hydrogel, we aimed at identifying the gel surface and extracting quantitative information about its deformation induced by the biofilms. In most cases, we used an automated data analysis pipeline as described below. To get an average profile of the deformation caused by the biofilms, we performed a radial reslice in Fiji over 180 degrees around the center of the deformation (one degree per slice). We then performed an average intensity projection of the obtained stack. Tocalculate the diameter of the biofilm, we averaged 4 measurements of the biofilm diameter taken at different angles. The resliced images were then imported in Matlab R2017a (Mathworks) as two-dimensional (x-y) matrices of intensities. In these images, the surface was consistently brighter than the rest of the gel. Therefore, we identified the surface profile as the pixels having the maximal intensity in each column of the matrix. Note that the bottom of the gel sometimes also comprised bright pixels that introduced noise in the profile. To reduce this problem, we thus excluded 20 rows at the bottom of each image (~3.7 µm). We then calculated the baseline position of our gel – namely, the height of the non-deformed portion of the gel. In our pictures, this corresponds to the height at the left and right extremities of the profile. Therefore, we defined the baseline as the average of the first 50 and last 50 pixels of the profile (~9 µm on each side of the profile). We then offset the whole picture so that the baseline position corresponded to y = 0. We undersampled the extracted surface profiles to further reduce noise, by keeping only the maximal y value over windows

of 40 pixels. Finally, we fitted a smoothing spline to the undersampled profile using the built-in *fit* function in Matlab, with a smoothing parameter value of 0.9999.

To quantify the deformation that biofilms induced on the hydrogel, we measured the amplitude ($\delta_{max}$) of the deformed peak and its full width at half maximum (λ). First, we evaluated the fitted profile described above at a range of points spanning the whole width of the picture and spaced by 0.0005 µm. We identified the maximal value of the profile at these points, which corresponds to the amplitude of the peak $\delta_{max}$ (with respect to the baseline, which is defined as y = 0). We then split the profile in two: one part on the left of the maximum, and one part on its right. On each side, we found the point on the profile whose y value was the closest to $0.5 \cdot \delta_{max}$ using the Matlab function *knnsearch*. We then calculated the distance between their respective x values, which corresponds to the λ of the deformed peak. Our data analysis program also included a quality control feature, which prompted the user to accept or reject the computed parameters. When imaging quality was insufficient to ensure proper quantification with our automated pipeline, we measured the deformation manually in Fiji.

*Digital volume correlation and traction force microscopy*

We performed particle tracking to measure local deformations and ultimately compute stress and traction forces within hydrogels as biofilms grew. To do this, we performed timelapse visualizations of the hydrogel during the formation of a biofilm at high spatial resolution with a 60X, NA 0.95 water immersion objective. We thus generated 200 µm x 200 µm x 25 µm (50 stacks of 1200x1200 pixels) volumes at 14 different time points. These images were subsequently registered to eliminate drift using the Correct 3D Drift function in Fiji. To compute local material deformations which we anticipated to generate large strains, we used an iterative Digital Volume Correlation (DVC) scheme [26]. These were performed with 128x128x64 voxel size in cumulative mode, meaning deformations are calculated by iterations between each time point over the whole 4D timelapse, rather than directly from the

reference initial image. The DVC code computes material deformation fields in 3D which we subsequently use as input for the associated large deformation traction force microscopy (TFM) algorithm [26]. The TFM calculates stress and strain fields given the material's Young modulus ($E$ = 38 kPa in our case) to ultimately generate a traction force map at the hydrogel surface.

## References


1. Flemming, H. C. & Wingender, J. The biofilm matrix. *Nat. Rev. Microbiol.* **8**, 623–633 (2010).

2. Donlan, R. M. & Costerton, J. W. Biofilms: Survival mechanisms of clinically relevant microorganisms. *Clinical Microbiology Reviews* **15**, 167–193 (2002).

3. Tischler, A. D. & Camilli, A. Cyclic diguanylate regulates Vibrio cholerae virulence gene expression. *Infect. Immun.* **73**, 5873–82 (2005).

4. Harris, A. R. *et al.* Characterizing the mechanics of cultured cell monolayers. *Proc. Natl. Acad. Sci. U. S. A.* **109**, 16449–16454 (2012).

5. Yan, J. *et al.* Mechanical instability and interfacial energy drive biofilm morphogenesis. *Elife* **8**, (2019).

6. Hartmann, R. *et al.* Emergence of three-dimensional order and structure in growing biofilms. *Nat. Phys.* **15**, 251–256 (2019).

7. Beroz, F. *et al.* Verticalization of bacterial biofilms. *Nat. Phys.* **14**, 954–960 (2018).

8. Duvernoy, M. C. *et al.* Asymmetric adhesion of rod-shaped bacteria controls microcolony morphogenesis. *Nat. Commun.* **9**, 25–28 (2018).

9. Timoshenko, S. & Gere, J. M. *Theory of elastic stability*. (Dover Publications, 2009).

10. Charras, G. & Yap, A. S. Tensile Forces and Mechanotransduction at Cell–Cell Junctions. *Curr. Biol.* **28**, R445–R457 (2018).

11. Rojas, E. R. & Huang, K. C. Regulation of microbial growth by turgor pressure. *Curr. Opin. Microbiol.* **42**, 62–70 (2018).

12. Discher, D. E., Janmey, P. & Wang, Y. Tissue Cells Feel and Respond to the Stiffness of Their Substrate. **310**, 1139–1144 (2005).

13. Lee, S., Tong, X. & Yang, F. The effects of varying poly(ethylene glycol) hydrogel crosslinking density and the crosslinking mechanism on protein accumulation in three-dimensional hydrogels. *Acta Biomater.* **10**, 4167–4174 (2014).

14. Wang, C. Y. On the Buckling of a Circular Plate on an Elastic Foundation. *J. Appl. Mech.* **72**, 795–796 (2005).

15. Teschler, J. K. *et al.* Living in the matrix: assembly and control of Vibrio cholerae biofilms. *Nat. Rev. Microbiol.* **13**, 255–268 (2015).

16. Jennings, L. K. *et al.* Pel is a cationic exopolysaccharide that cross-links extracellular DNA in the Pseudomonas aeruginosa biofilm matrix. **112**, 11353–11358 (2015).

17. Kovach, K. *et al.* Evolutionary adaptations of bio fi lms infecting cystic fi brosis lungs promote mechanical toughness by adjusting polysaccharide production. (2016). doi:10.1038/s41522-016-0007-9

18. Colvin, K. M. *et al.* The Pel and Psl polysaccharides provide Pseudomonas aeruginosa structural redundancy within the biofilm matrix. *Environ. Microbiol.* **14**, 1913–28 (2012).

19. Wang, Q. & Zhao, X. A three-dimensional phase diagram of growth-induced surface instabilities. *Sci. Rep.* **5**, 8887 (2015).

20. Swidsinski, A. *et al.* Presence of a Polymicrobial Endometrial Biofilm in Patients with

Bacterial Vaginosis. *PLoS One* **8**, e53997 (2013).

21. Hardy, L. *et al.* A fruitful alliance: the synergy between Atopobium vaginae and Gardnerella vaginalis in bacterial vaginosis-associated biofilm. *Sex. Transm. Infect.* **92**, 487–491 (2016).

22. Engel, P., Bartlett, K. D. & Moran, N. A. The Bacterium Frischella perrara Causes Scab Formation in the Gut of its Honeybee Host. *MBio* **6**, e00193-15 (2015).

23. Chelakkot, C., Ghim, J. & Ryu, S. H. Mechanisms regulating intestinal barrier integrity and its pathological implications. *Exp. Mol. Med. 2018 508* **50**, 1–9 (2018).

24. Pestrak, M. J. *et al.* Pseudomonas aeruginosa rugose small-colony variants evade host clearance, are hyper-inflammatory, and persist in multiple host environments. *PLOS Pathog.* **14**, e1006842 (2018).

25. Fong, J. C. N., Karplus, K., Schoolnik, G. K. & Yildiz, F. H. Identification and characterization of RbmA, a novel protein required for the development of rugose colony morphology and biofilm structure in Vibrio cholerae. *J. Bacteriol.* **188**, 1049–59 (2006).

26. Toyjanova, J. *et al.* High Resolution, Large Deformation 3D Traction Force Microscopy. *PLoS One* **9**, e90976 (2014).

27. Berk, V. *et al.* Molecular architecture and assembly principles of Vibrio cholerae biofilms. *Science* **337**, 236–9 (2012).

28. Yildiz, F. H., Liu, X. S., Heydorn, A. & Schoolnik, G. K. Molecular analysis of rugosity in a Vibrio cholerae O1 El Tor phase variant. *Mol. Microbiol.* **53**, 497–515 (2004).

29. Hickman, J. W., Tifrea, D. F. & Harwood, C. S. A chemosensory system that regulates biofilm formation through modulation of cyclic diguanylate levels. *Proc. Natl. Acad. Sci. U. S. A.* **102**, 14422–7 (2005).

30. Rybtke, M. T. *et al.* Fluorescence-based reporter for gauging cyclic di-GMP levels in Pseudomonas aeruginosa. *Appl. Environ. Microbiol.* **78**, 5060–9 (2012).

31. Rybtke, M. *et al.* The LapG protein plays a role in Pseudomonas aeruginosa biofilm formation by controlling the presence of the CdrA adhesin on the cell surface. *Microbiologyopen* **4**, 917–30 (2015).

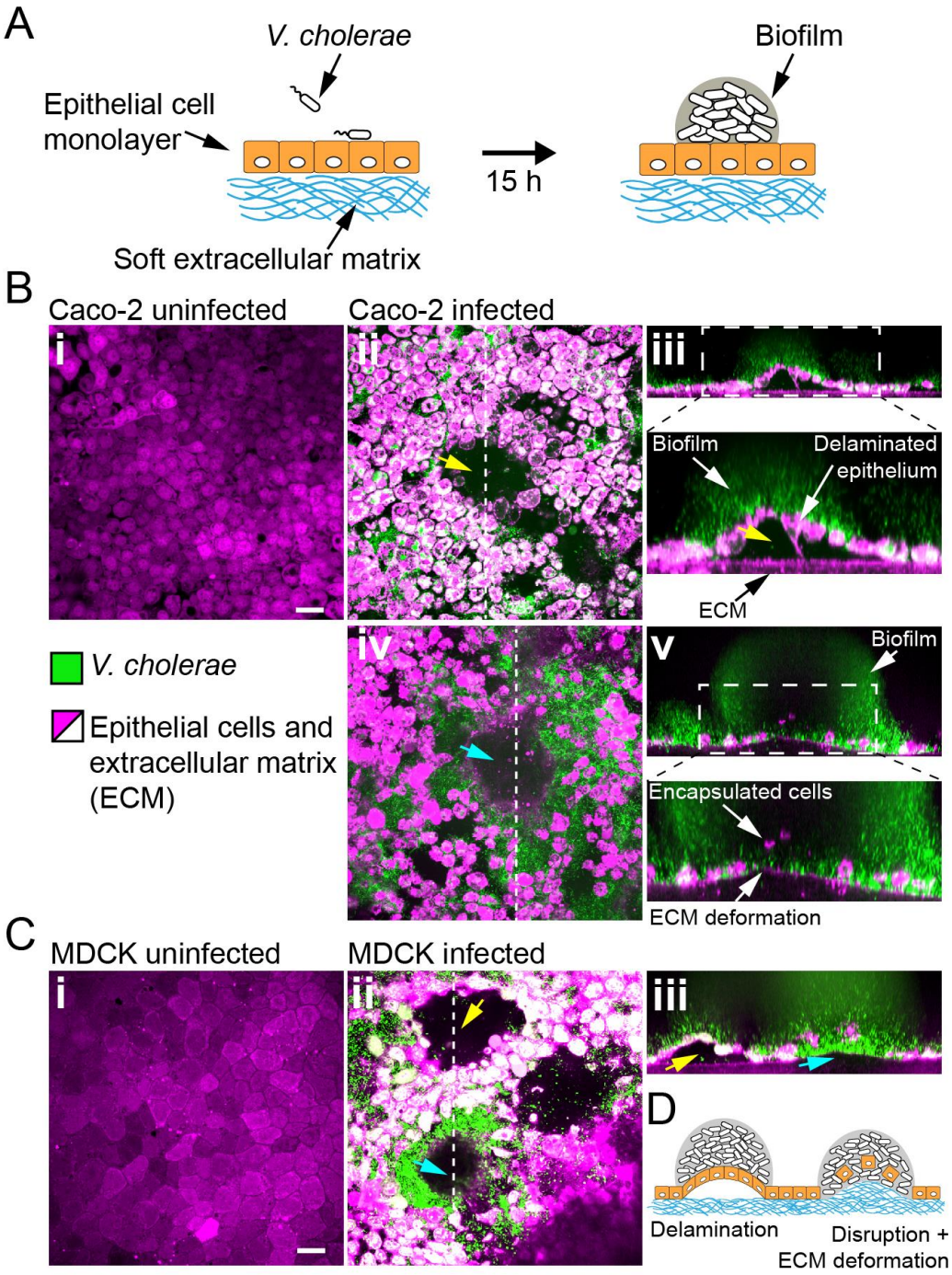


**Fig. 1: Biofilms deform and disrupt epithelial cell monolayer.** (A) Caco-2 and MDCK cells grow at the surface of a soft ECM into a tight monolayer on which we seed a liquid inoculum of *V. cholerae*. (B) Confocal images of uninfected (i) and infected (ii-v) monolayers of Caco-2 cells. Yellow arrow indicates gaps in the epithelial monolayer (ii and iii), blue arrow shows deformed ECM (iv). (C) Confocal images of uninfected (i) and infected (ii-iii)

monolayers of MDCK cells, also showing delamination and rupture as illustrated in (D). Scale bars: 20 µm.

428

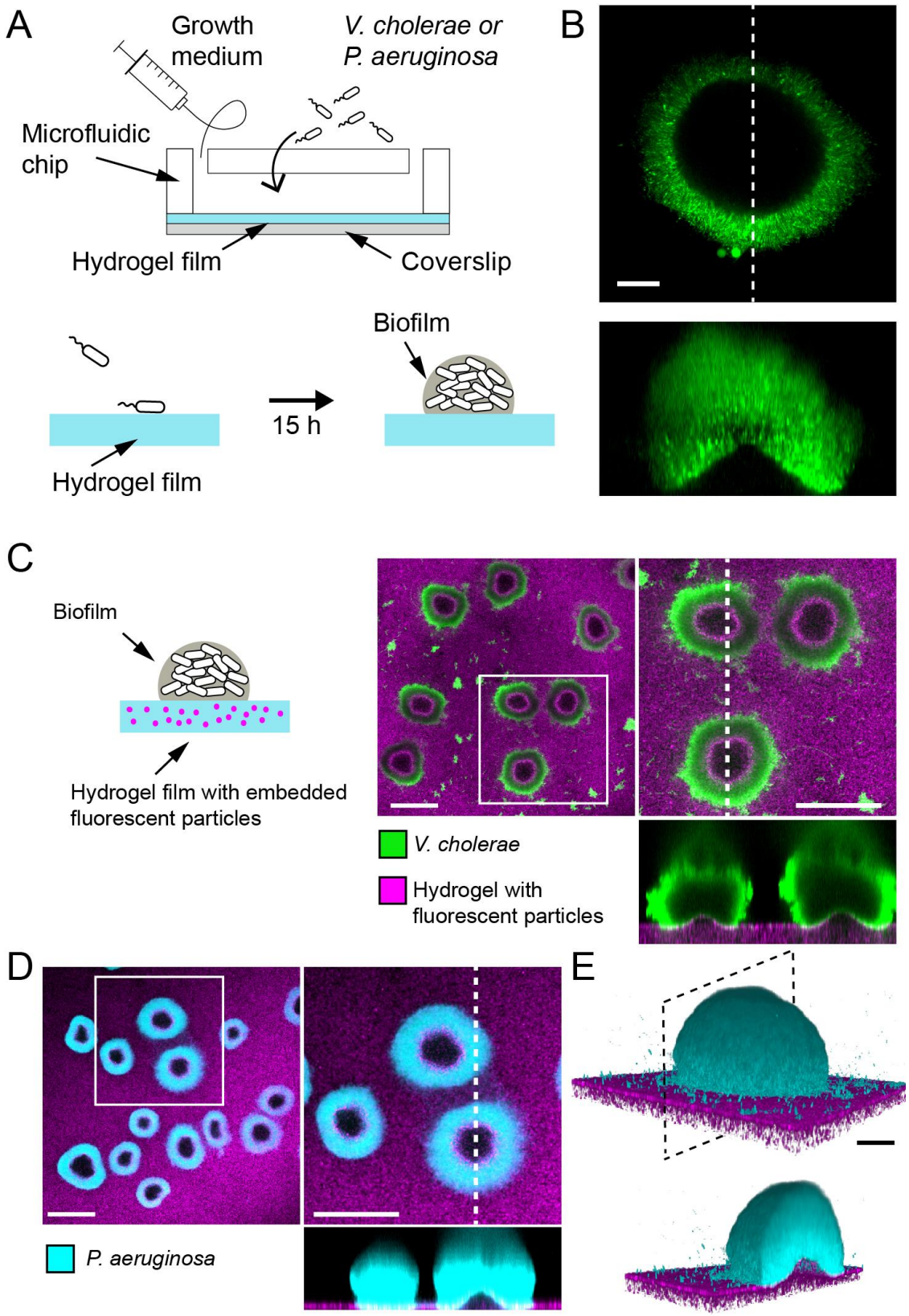
A
Growth medium
V. cholerae or P. aeruginosa
Microfluidic chip
Hydrogel film
Coverslip
Biofilm
15 h
Hydrogel film
B
C
Biofilm
Hydrogel film with embedded fluorescent particles
V. cholerae
Hydrogel with fluorescent particles
D
P. aeruginosa
E

429

**Fig. 2: Biofilms deform soft substrates.** (A) Thin hydrogel films at the bottom surface of microchannels reproduce the mechanical properties of host tissues. (B) Confocal visualizations show that *V. cholerae* biofilms growing on hydrogels display large gaps at their core. (C) *V. cholerae* biofilms formed at the surface of hydrogels containing fluorescent particles. (D) *P. aeruginosa* biofilms similarly deform the soft substrates. Hydrogel elastic modulus: (B and C) E= 12 kPa , (D and E) E = 38 kPa.  Scale bars: (C and D) 100 µm, (B and E) 20 µm.

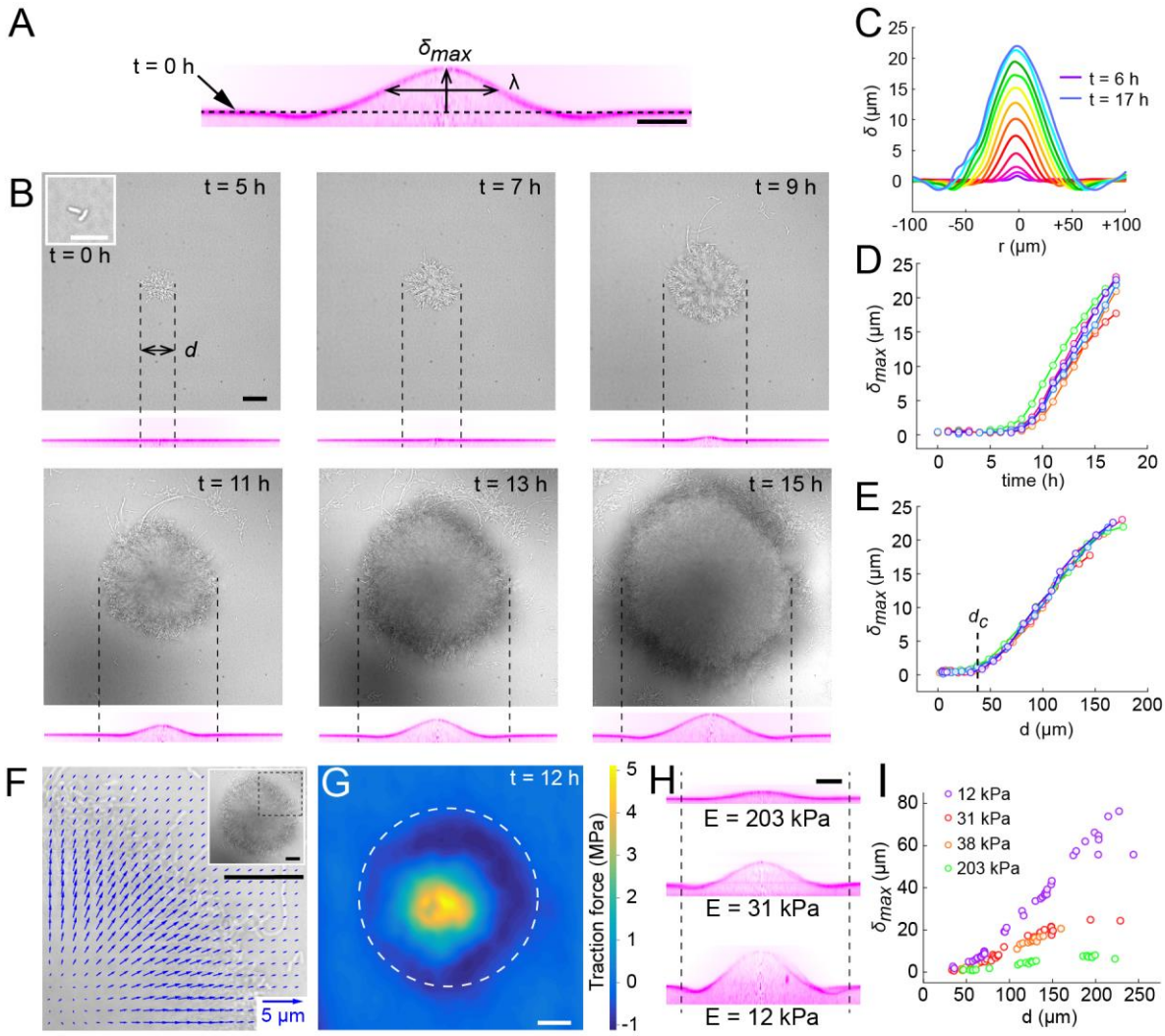


**Fig. 3: Biofilm buckle to deform their growth substrate.** (A) Morphological parameters $\delta_{max}$ (maximum deformation amplitude) and $\lambda$ (half max full width) computed from resliced deformation profiles. Dashed line indicates the baseline position of the gel surface. (B) Timelapse visualization of deformation (reslice, bottom) with biofilm growth (brightfield, top). Dashed lines indicate biofilm position and size on hydrogel profile. (C) Superimposition of these profiles shows the rapid deformation and the emergence of a recess at biofilm edges after 15 h. Each color corresponds to a different biofilm. (D) Biofilm age-dependence of $\delta_{max}$. (E) The dependence of $\delta_{max}$ on biofilm diameter highlights a critical biofilm diameter $d_c$ above which deformation occurs. (F) Hydrogel deformation field computed between 11 h and 12 h of growth, superimposed with a brightfield image of the biofilm. Data represented

for the top right quarter of the biofilm shown in inset (dashed lines). (G) traction force measurements at the deformation surface. The dashed line shows the edge of the biofilm. (H) Deformation profiles on three hydrogels with different stiffness for biofilms of equal diameter. (I) Biofilm diameter-dependence of maximum deformation for four different hydrogel stiffnesses matching tissue properties. Scale bar: 10 µm for inset $t$ = 0 h in (B), else 20 µm.

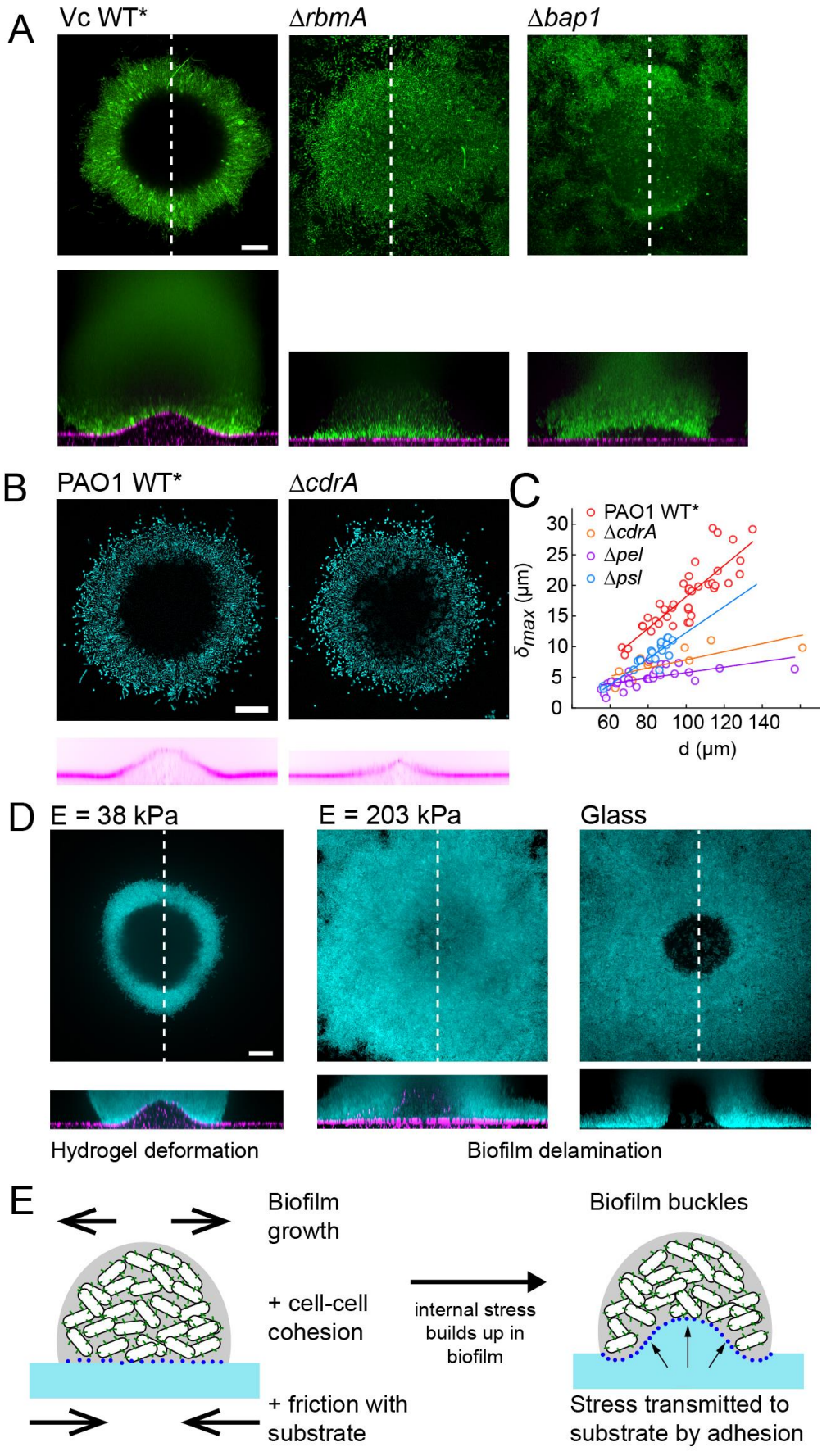
A
Vc WT*
ΔrbmA
Δbap1
B
PAO1 WT*
ΔcdrA
C
PAO1 WT*
ΔcdrA
Δpel
Δpsl
δmax (μm)
d (μm)
D
E = 38 kPa
E = 203 kPa
Glass
Hydrogel deformation
Biofilm delamination
E
Biofilm growth
+ cell-cell cohesion
+ friction with substrate
internal stress builds up in biofilm
Biofilm buckles
Stress transmitted to substrate by adhesion

461

**Fig. 4: Biofilm mechanical properties and adhesion drive substrate deformation.** (A) Deformations of hydrogel substrates by *V. cholerae* WT*, Δ*rbma* and Δ*bap1* biofilms. (B) Deformations of hydrogels by *P. aeruginosa* WT* and Δ*cdrA* biofilms. (C) Dependence of maximum deformations on *P. aeruginosa* WT*, Δ*cdrA*, Δ*pel* and Δ*psl* biofilm diameter. (D) Increasing hydrogel stiffness to 200 kPa induces delamination of biofilms, as observed on glass. (E) A model for biofilm deformation of soft substrates. Scale bars: 20 µm.

**Table 1.** Plasmids and strains used in this study

| Strain or plasmid | Relevant genotype | Source |
|---|---|---|
| pFY_113 | plasmid for generation of in-frame *rbmA* deletion mutants | [27] |
| pFY_330 | plasmid for generation of in-frame *bap1* deletion mutants | [27] |
| V. cholerae O1 El Tor A1552 (Vc WT*) | rugose variant | [28] |
| V. cholerae ΔrbmA | in frame deletion of Rbma in rugose backgrounds | This study |
| V. cholerae Δbap1 | in frame deletion of Bap1 in rugose backgrounds | This study |
| PAO1 WT | wild-type, $Gm^r$ | [29] |
| PAO1ΔwspF (PAO1 WT*) | in frame deletions of WspF, $Gm^r$ | [30] |
| PAO1ΔwspFΔpel | in frame deletions of WspF, PelA genes, $Gm^r$ | [30] |
| PAO1ΔwspFΔpsl | in frame deletions of WspF, PslBCD genes, $Gm^r$ | [30] |
| PAO1ΔwspFΔcdrA | in frame deletions of WspF, PslBCD, cdrA genes, $Gm^r$ | [31] |

**Table 2.** Molecular weight and concentrations of the precursors used for the generation of the hydrogels and resulting elastic modulus

| Precursor | Concentration wt/vol | Modulus kPa |
|---|---|---|
| PEGDA MW 10000 (Biochempeg) | 10% | 12.1 ± 0.8 |
| PEGDA MW 6000 (Biochempeg) | 10% | 38.3 ± 1.0 |
| PEGDA MW 3400 (Biochempeg) | 10% | 30.9 ± 2.0 |
| PEGDA MW 700 (Sigma-Aldrich) | 15% | 203.3 ± 13.7 |